Proceedings of ALGORITMY 2016
pp. 33–43

DISCRETE DUALITY FINITE VOLUME METHOD FOR MEAN CURVATURE FLOW OF SURFACES*

L. TOMEK†, K. MIKULA†, AND M. REMEŠÍKOVÁ†

Abstract. In this paper we propose a new numerical method for solving the mean curvature flow of surfaces. Two-dimensional surface is usualy approximated by a triangular mesh. Widely used discretization of Laplace-Beltrami operator over triangulated surfaces is the so-called cotangent scheme [7, 8]. In the cotangent scheme the unknowns are the vertices of the triangulation. The basic idea of our new approach is to include a representative point of each triangle (vertex of the dual mesh) in the scheme as a supplementary unknown and generalize the discrete duality finite volume method [3] from R^2 to 2D surfaces embedded in R^3. We derive the numerical scheme and present numerical experiments illustrating the basic properties of the method.

Key words. surface evolution, mean curvature flow, finite volume, discrete duality

AMS subject classifications. 53A10, 65D17, 65M08

1. Introduction. Let $\varphi^0 : M \to R^3$ be a smooth embedding of a 2-dimensional manifold M in Euclidean space. The evolution of $M^0 = \varphi^0(M)$ by the mean curvature flow is a one-parameter family of embeddings $\varphi : M \times [0, t_f] \to R^3$ satisfying

$$\partial_t \varphi(X,t) = H(X,t)N(X,t) \quad \text{with} \quad \varphi(X,0) = \varphi^0(X), \tag{1.1}$$

where $H(X,t)$ and $N(X,t)$ are respectively the mean curvature and the unit normal of the surface $M^t = \varphi^t(M)$ at the point $X \in M$, where $\varphi^t = \varphi(\cdot, t)$, see Fig. 1.1. The mean curvature at given point is the sum of the principal curvatures, $H = \kappa_{\max} + \kappa_{\min}$. The quantity $h(X,t) = H(X,t)N(X,t)$ is called mean curvature vector.

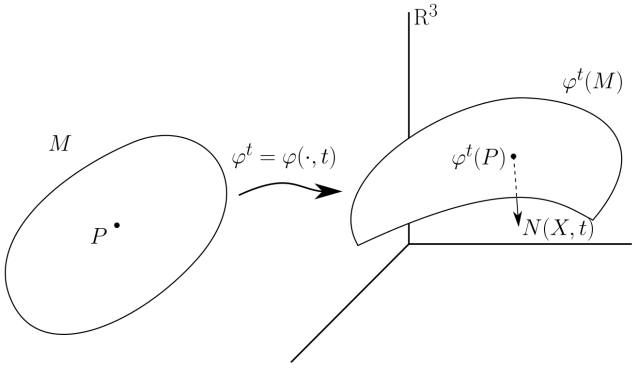

FIG. 1.1. *Evolving surface from differential geometry viewpoint.*

For a surface with boundary, the model (1.1) is coupled with a Dirichlet boundary condition

$$\varphi(X,t) = \varphi^0(X), \qquad X \in \partial M. \tag{1.2}$$

*This work was supported by projects VEGA 1/0608/15, VEGA 1/0728/15 and APVV-0072-11.

†Faculty of Civil Engineering, Slovak University of Technology, Radlinského 11, 810 05 Bratislava, Slovak Republic (tomek@math.sk, mikula@math.sk, remesikova@math.sk).

Using the formula $h = \triangle_{g_\varphi}\varphi$ (see [6]) we can rewrite the model (1.1) to the form

$$\partial_t\varphi = \triangle_{g_\varphi}\varphi \quad \text{with} \quad \varphi(X,0) = \varphi^0(X). \tag{1.3}$$

The symbol $\triangle_{g_\varphi}$ denotes the Laplace-Beltrami operator associated with the metric tensor g_φ induced by the embedding φ^t (we use abbreviation g_φ for g_{φ^t}).

The numerical methods for solving the equation (1.3) are usually based on a finite element method [1, 4] or a finite volume method [7, 8]. In this work we deal with a finite volume method. Given a (primal) mesh, finite volume methods for the equation (1.3) may be classified into two main distinct categories: "vertex-centered"[1] and "cell-centered"[2] methods. For a review of these methods, we refer to [5].

In the paper [2] the authors study a specific cell-centered method, the so-called diamond-cell method. A diamond cell is a quadrilateral cell associated with a side of the primal mesh and is obtained by joining the two vertices of this side with the centers of the two cells of the primal mesh which share this side. The mean value of $\nabla\varphi$ is defined using the values of φ at the centers and at the vertices of the primal cells. The discrete solution at the vertices of the primal mesh is computed by an interpolation of its values at the centers of the neighboring cells.

In the paper [3] the authors develop a discrete duality finite volume (DDFV) method which is a fusion of the vertex-centered and cell-centered approach. They adopt the diamond-mesh technique to reconstruct $\nabla\varphi$, but instead of interpolating the values of φ at the vertices of the primal mesh, they consider these values as supplementary unknowns of the numerical scheme.

In this work we generalize the DDFV from R^2 to 2D surfaces embedded in R^3. The motivation for a new finite volume method for the mean curvature flow rises also from the fact that the finite volumes in the widely used vertex-centered method, the so-called cotangent scheme [8], are not defined uniquely in the following sense: the "cell center" of a triangle (cell of the primal mesh) used for the construction of the finite volume (cell of the dual mesh) can lie anywhere in the triangle and the integral of the term $\triangle_{g_\varphi}\varphi$ in (1.3) over the finite volume is the same. Since, in the discrete differential geometry [8], the mean curvature vector is then approximated by dividing the integral by the area of the finite volume, it may lead to arbitrary number depending on the choice of the "cell center". In our scheme we reduce this non-uniqueness by including the cell centers to unknowns.

2. Discretization of mean curvature flow. In this section we perform a discretisation of (1.3) by a new discrete duality finite volume (DDFV) method.

2.1. Time discretization. In order to discretize (1.3) in the time domain, the semi-implicit approach is used. The time derivative is approximated by a finite difference and the Laplace-Beltrami operator is taken from the previous time step. If τ is the time step, $N = t_f/\tau$ is the number of time steps, $t^n = n\tau$ and $\varphi^n = \varphi(\cdot, t^n)$, we obtain

$$\frac{\varphi^n - \varphi^{n-1}}{\tau} = \triangle_{\varphi^{n-1}}\varphi^n \tag{2.1}$$

for $n = 1, \ldots, N$, where the symbol $\triangle_{\varphi^{n-1}}$ denotes the Laplace-Beltrami operator from the previous time step with respect to the metric $g_{\varphi^{n-1}}$ induced by φ^{n-1}.

[1] Computing approximate values of φ at the vertices of the primal mesh

[2] Computing approximate values of φ at the centers of the cells of the primal mesh.

2.2. Space discretization.

2.2.1. Triangular mesh. The construction of a mesh for DDFV method is based on the triangular mesh used in cotangent scheme [8]. It considers a triangulation $\bar{M}$ of the manifold M, which is a simplical complex homeomorphic to M. Corresponding homeomorphism $\rho : \bar{M} \to M$ induces a triangular structure on M consisting of vertices $X_i = \rho(\bar{X}_i)$, $i = 1, \dots, n_F$, edges e_j, $j = 1, \dots, n_E$ and triangles $\mathcal{T}_p$, $p = 1, \dots, n_T$, where $\bar{X}_i$, $i = 1, \dots, n_F$ are the vertices of the triangulation $\bar{M}$. The surface $M^n = \varphi^n(M)$ is also endowed with a triangular structure induced by the

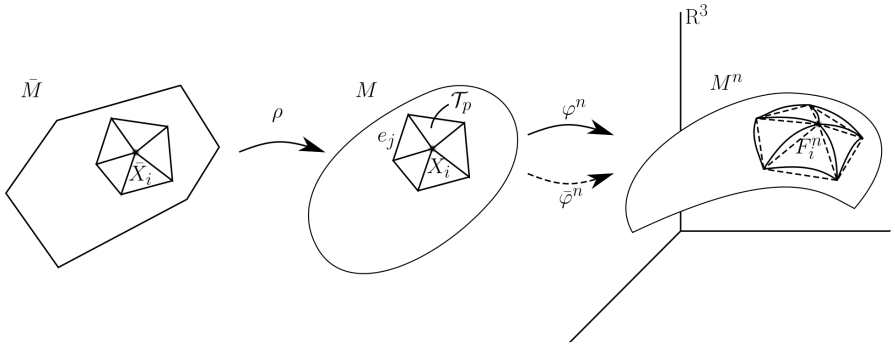

FIG. 2.1. *Triangulated surface from the point of view of the differential geometry.*

map $\varphi^n \circ \rho$ (Fig. 2.1, sketched by solid lines). An approximation of M^n is defined using a new embedding $\bar{\varphi}^n : M \to R^3$ which is linear on each triangle $\mathcal{T}_{i,p}$. The surface $\bar{M}^n = \bar{\varphi}^n(M)$ is a polyhedral approximation of M^n (Fig. 2.1, sketched by dashed lines) with vertices $F_i^n = \varphi^n(X_i) = \bar{\varphi}^n(X_i)$, edges $e_j^n = \bar{\varphi}^n(e_j)$ and triangular faces $\mathcal{T}_p^n = \bar{\varphi}^n(\mathcal{T}_p)$.

The finite volume mesh is constructed by the barycentric subdivision of M. The finite volume (or covolume) V_i around a vertex X_i is a region bounded by the piecewise linear curve joining the barycenters of the neighbouring triangles and the midpoints of the edges leading to the neighbouring vertices $X_{i,p}$, $p = 1, \dots, m$ where m is the number of neighbours.

2.2.2. Diamond mesh. In our approach we modify the mesh $\bar{M}^n$ used in the cotangent scheme. We create a representative point T_i^n of each triangle $\mathcal{T}_i^n$ (Fig. 2.2, left). The point T_i^n does not need to lie in the triangle, only its projection to $\mathcal{T}_i^n$ does. The vertices F_i^n and T_i^n will be referred to as F-vertices and T-vertices respectively.

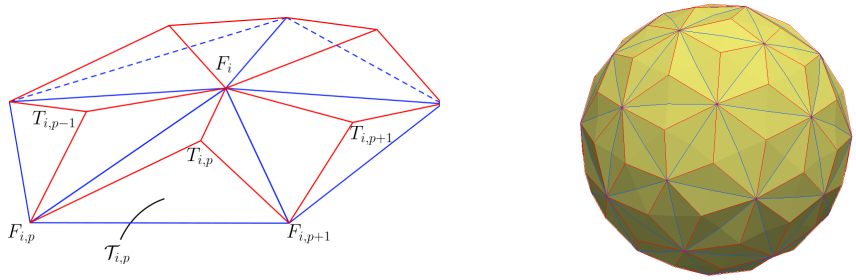

FIG. 2.2. *Left, the edges of the original mesh (blue lines) and the edges of the diamond mesh (red lines) in the neighbourhood of the vertex F_i. Right, the diamond mesh (red lines) on the sphere.*

Next, the triangular mesh is replaced by a diamond mesh. The edges of the diamond mesh are the line segments joining each F-vertex with all neighbouring T-vertices (Fig. 2.2). For a manifold with boundary the edges connecting boundary F-vertices

are also included to the diamond mesh (Fig. 2.3, right). The basic geometric object is a diamond cell, denoted by V^D, which is a surface patch bounded by four edges (Fig. 2.4). For a manifold with boundary the boundary diamond cells V^D are triangles with two F-vertices and one T-vertex (Fig. 2.3, right).

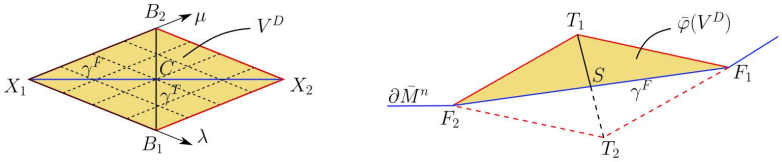

FIG. 2.3. *Left, local coordinates on an inner diamond cell on M. Right, a boundary diamond cell on $\bar{M}^n$.*

The manifold $\bar{M}$ and the homeomorphism $\rho : \bar{M} \to M$ are changed analogously. The homeomorphism ρ induces a new structure on M with vertices X_i, $i = 1, \ldots, n_F$ and B_i, $i = 1, \ldots, n_T$. For the embedding $\bar{\varphi}^n : M \to R^3$ of a diamond cell V^D with vertices X_1, B_1, X_2, B_2 we use a bilinear interpolation

$$\bar{\varphi}^n(X) = (1-\lambda)(1-\mu)F_1^n + \lambda\mu F_2^n + \lambda(1-\mu)T_1^n + (1-\lambda)\mu T_2^n, \quad X \in V^D, \tag{2.2}$$

where $T_i^n = \varphi^n(B_i)$, $F_i^n = \varphi^n(X_i)$ and $\lambda, \mu \in [0,1]$ are the local coordinates of a point $X \in V^D$ (Fig. 2.3, left). Geometric quantities needed in following computations are denoted in Fig. 2.4 and will be defined properly later. The center C of an inner diamond cell V^D is defined by $\bar{\varphi}^n(C) = \frac{1}{4}(F_1^n + T_1^n + F_2^n + T_2^n) = S$. If V^D is a

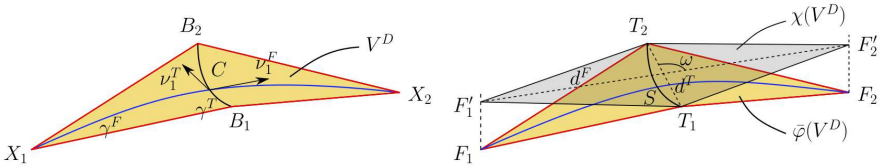

FIG. 2.4. *The geometry of a diamond cell. Left, a diamond cell on the manifold M. Right, $\bar{\varphi}$-image of a diamond cell on $\bar{M}^n$.*

boundary diamond cell, the equation (2.2) reduces to a linear interpolation.

Resulting mesh consists of $n_V = n_F + n_T$ vertices and $n_{dia} = \frac{3}{2}n_T$ diamond cells (in case of closed manifold[3]). Our diamond mesh is a generalization of 2D planar diamond mesh used in DDFV method developed in [3] to 2D surfaces in R^3.

2.2.3. Induced metric $g_{\bar{\varphi}^n}$. For the derivation of the numerical scheme we need the expression for the induced metric $g_{\bar{\varphi}^n}$ at the center C of a diamond cell V^D. To obtain the induced metric $g_{\bar{\varphi}^n}$, the standard Euclidean metric is pushed back from R^3 to M by the map $\bar{\varphi}$ and evaluated at the center C (i.e. $(\lambda, \mu) = \left(\frac{1}{2}, \frac{1}{2}\right)$). The resulting expression is (in the matrix form)

$$g^C_{\bar{\varphi}^n} \leftrightarrow \frac{1}{4}\begin{pmatrix} \|u-v\|^2 & (u-v)\cdot(u+v) \\ (u-v)\cdot(u+v) & \|u+v\|^2 \end{pmatrix}, \tag{2.3}$$

where $u = F_2 - F_1$, $v = T_2 - T_1$, see [9] for details.

2.2.4. Equations for F-vertices. The finite volume V_i^F around the vertex X_i is a region bounded by a curve joining the neighbouring vertices $B_{i,p}$ and the centers $C_{i,p}$ of the diamond cells $V_{i,p}^D$, $p = 1, \ldots, m$ (Fig. 2.5, left). The part of the boundary between $B_{i,p-1}$ and $B_{i,p}$ is a curve $\gamma_{i,p}^T : (\lambda(t), \mu(t)) = (1-t, t), t \in [0,1]$ (by convention, X_i is the origin of the local coordinate system on each $V_{i,p}^D$).

[3]For a manifold with boundary $n_{dia} > \frac{3}{2}n_T$ and n_{dia} approaches $\frac{3}{2}n_T$ as the mesh size decreases.

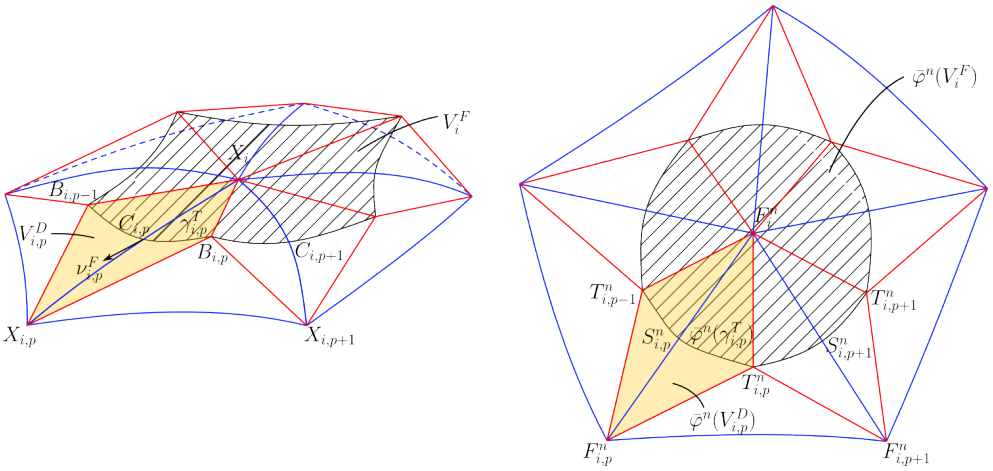

FIG. 2.5. *Left, the finite volume V_i^F around the vertex $X_i \in M$. Right, the notation in the neighbourhood of the vertex $F_i^n = \bar\varphi^n(X_i) \in \bar M^n$.*

To obtain the equation for F_i^n we integrate (2.1) over V_i^F, with φ^n being replaced by its piecewise bilinear approximation $\bar\varphi^n$. We obtain (using the divergence theorem)

$$\chi^{n-1}(V_i^F)\frac{F_i^n - F_i^{n-1}}{\tau} = \sum_{p=1}^{m} \int\limits_{\gamma_{i,p}^T} g_{\bar\varphi^{n-1}}\left(\nabla_{\bar\varphi^{n-1}}\bar\varphi^n, \nu_{i,p}^{n-1}\right) d\xi^{n-1}, \tag{2.4}$$

where $\nu_{i,p}^{n-1}$ is the outward unit normal to the covolume V_i^F on the curve $\gamma_{i,p}^T$. The area of the covolume $\chi(V_i^F)$ is approximated by the total area of $2m$ triangles with vertices $F_i, S_{i,p}, T_{i,p}$ and $F_i, T_{i,p}, S_{i,p+1}$ (Fig. 2.5, right) for $p = 1, \dots, m$ (by convention, $S_{i,m+1} = S_{i,1}$). Note that the equation (2.4) is a vector one, thus for each i we have 3 scalar equations.

Calculation of the integral over $\gamma_{i,p}^T$. We approximate the value of the integral in (2.4) using the value in the center $C_{i,p}$. To simplify the notation we omit most of indices i and n throughout this section.

$$\int\limits_{\gamma_p^T} g_{\bar\varphi}\left(\nabla_{\bar\varphi}\bar\varphi, \nu_p\right) d\xi \approx \left|\gamma_p^T\right| g_{\bar\varphi}^{C_p}\left(\nabla_{\bar\varphi}\bar\varphi(C_p), \nu_p^F\right), \tag{2.5}$$

where $|\gamma_p^T| = \|T_{p-1} - S_p\| + \|T_i - S_p\|$ is the approximate length of γ_p^T and $\nu_p^F = \nu_p(C_p)$ is the outward unit normal to ∂V_i^F at point C_p. The tangent vector to γ_p^T at point C_p is $\dot\gamma_p^T = -\partial_\lambda + \partial_\mu$. We obtain a formula for the normal $\nu_p^F = (\nu_p^F)^\lambda \partial_\lambda + (\nu_p^F)^\mu \partial_\mu$ after using conditions $g_{\bar\varphi^n}^{C_p}(\dot\gamma_p^T, \nu_p^F) = 0$ (orthogonality), $g_{\bar\varphi^n}^{C_p}(\nu_p^F, \nu_p^F) = 1$ (normalization) and $(\nu_p^F)^\lambda, (\nu_p^F)^\mu > 0$ (correct orientation) in the following form

$$\nu_p^F = \frac{\|v\|^2 + u\cdot v}{\|v\|\sqrt{\|u\|^2\|v\|^2 - (u\cdot v)^2}}\partial_\lambda + \frac{\|v\|^2 - u\cdot v}{\|v\|\sqrt{\|u\|^2\|v\|^2 - (u\cdot v)^2}}\partial_\mu, \tag{2.6}$$

where $u = F_{i,p} - F_i$, $v = T_{i,p} - T_{i,p-1}$, see [9] for details. From (2.2) we evaluate the derivatives of the embedding in the center of the diamond cell

$$\partial_\lambda\bar\varphi(C_p) = \frac{1}{2}(u - v), \qquad \partial_\mu\bar\varphi(C_p) = \frac{1}{2}(u + v). \tag{2.7}$$

Using the formula $g_{\bar\varphi}\left(\nabla_{\bar\varphi}\bar\varphi, \nu_p\right) = \nu_p^\lambda \partial_\lambda \bar\varphi + \nu_p^\mu \partial_\mu \bar\varphi$ and the equations (2.7), (2.6) the integral (2.5) follows

$$\int\limits_{\gamma_p^T} g_{\bar\varphi}\left(\nabla_{\bar\varphi}\bar\varphi, \nu_p\right) d\xi = \frac{\left|\gamma_p^T\right| d_p^T}{2\chi(V_p^D)}(F_{i,p} - F_i) - \frac{\left|\gamma_p^T\right|}{d_p^T}\cot\omega_p(T_{i,p} - T_{i,p-1}), \tag{2.8}$$

where $d_p^T = \|T_{i,p} - T_{i,p-1}\|$ is the distance between T-vertices of the diamond cell $V_{i,p}^D$, the area $\chi(V_p^D) = \frac{1}{2}\sqrt{\|u\|^2\|v\|^2 - (u\cdot v)^2} = \frac{1}{2}\|u \times v\|$ can be interpreted as the approximate measure of the diamond cell calculated as the area of the quadrangle with vertices F_1', T_1, F_2', T_2 (Fig. 2.4, right) which we get by shifting the line segment F_1F_2 in the direction of the vector $u \times v$ until it intersects the segment T_1T_2 and ω_p is the angle between $F_1'F_2'$ and T_1T_2.

Final equations. We use (2.8) on the right-hand side of (2.4) and reorder the sum (replace p by $(p+1)$ in the term containing $T_{i,p-1}$). The formula for the discretization of the Laplace-Beltrami operator follows

$$\begin{aligned}\int\limits_{V_i^F} \triangle_{\bar\varphi}\bar\varphi\, d\chi = &-\frac{1}{2}\sum_{p=1}^m \frac{\left|\gamma_{i,p}^T\right| d_{i,p}^T}{\chi(V_{i,p}^D)} F_i + \frac{1}{2}\sum_{p=1}^m \frac{\left|\gamma_{i,p}^T\right| d_{i,p}^T}{\chi(V_{i,p}^D)} F_{i,p} \\ &- \sum_{p=1}^m \left(\frac{\left|\gamma_{i,p}^T\right|}{d_{i,p}^T}\cot\omega_{i,p} - \frac{\left|\gamma_{i,p+1}^T\right|}{d_{i,p+1}^T}\cot\omega_{i,p+1}\right) T_{i,p}.\end{aligned} \tag{2.9}$$

We combine (2.4) with (2.9) and obtain the equations for F-vertices

$$a_i^{n-1}F_i^n + \sum_{p=1}^m b_{i,p}^{n-1}F_{i,p}^n + \sum_{p=1}^m c_{i,p}^{n-1}T_{i,p}^n = F_i^{n-1} \tag{2.10}$$

for $i = 1, \ldots, n_F$ and $n = 1, \ldots, N$, where

$$a_i = 1 + \tfrac{\tau}{2\chi(V_i^F)}\sum_{p=1}^m q_{i,p}^F, \quad b_{i,p} = -\tfrac{\tau}{2\chi(V_i^F)}q_{i,p}^F, \quad c_{i,p} = \tfrac{\tau}{\chi(V_i^F)}\left(q_{i,p}^T - q_{i,p+1}^T\right) \tag{2.11}$$

for $p = 1, \ldots, m$ and where $q_{i,m+1} = q_{i,1}$ and

$$q_{i,p}^F = \frac{\left|\gamma_{i,p}^T\right| d_{i,p}^T}{\chi(V_{i,p}^D)}, \qquad q_{i,p}^T = \frac{\left|\gamma_{i,p}^T\right|}{d_{i,p}^T}\cot\omega_{i,p}. \tag{2.12}$$

To reduce the complexity of notation we omitted the time step index n in (2.11) and (2.12). All geometric quantities in (2.11) and (2.12) are calculated from the $(n-1)$-th time step.

In case of the surface with boundary (1.2) we fix each boundary vertex $F_i^n \in \partial\bar M^n$ by replacing the corresponding equation (2.10) with $F_i^n = F_i^{n-1}$.

2.2.5. Equations for T-vertices. We construct the finite volume V_i^T around the vertex B_i (Fig. 2.6) as a region bounded by the curves $\gamma_{i,p}^F : (\lambda(t), \mu(t)) = (1 - t, 1 - t), t \in [0, 1]$, for $p = 1, 2, 3$ (by convention, $X_{i+1,p}$ is the origin of the local coordinate system on each $V_{i,p}^D$).

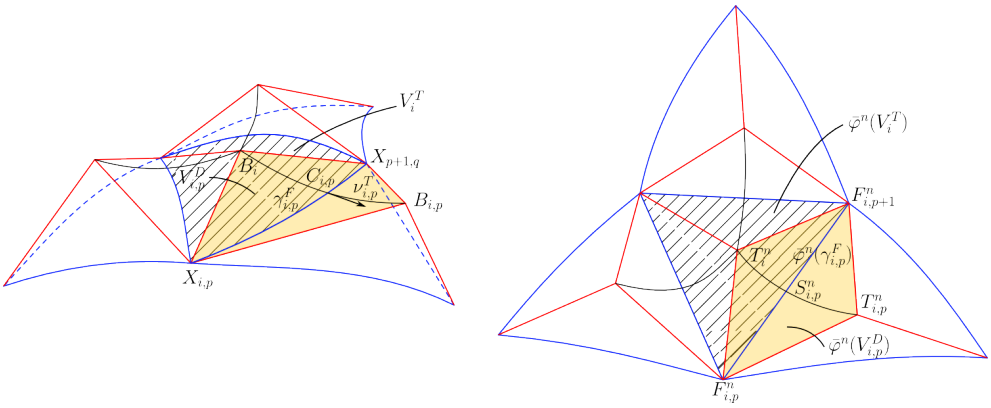

FIG. 2.6. *Left, the finite volume V_i^T around the vertex $B_i \in M$. Right, the notation in the neighbourhood of the vertex $T_i^n = \bar\varphi^n(B_i) \in \bar M^n$.*

Using a procedure analogous to the one presented in section 2.2.5 we obtain the equations for T-vertices (see [9] for details)

$$\hat a_i^{n-1} T_i^n + \sum_{p=1}^{3} \hat b_{i,p}^{n-1} T_{i,p}^n + \sum_{p=1}^{3} \hat c_{i,p}^{n-1} F_{i,p}^n = T_i^{n-1} \tag{2.13}$$

for $i = 1, \dots, n_T$ and $n = 1, \dots, N$, where

$$\hat a_i = 1 + \tfrac{\tau}{2\chi(V_i^T)} \sum_{p=1}^{3} \hat q_{i,p}^T, \quad \hat b_{i,p} = -\tfrac{\tau}{2\chi(V_i^T)} \hat q_{i,p}^T, \quad \hat c_{i,p} = \tfrac{\tau}{\chi(V_i^T)} \left(\hat q_{i,p}^F - \hat q_{i,p-1}^F \right) \tag{2.14}$$

for $p = 1, 2, 3$ and where $\hat q_{i,0} = \hat q_{i,3}$ and

$$\hat q_{i,p}^T = \frac{|\gamma_{i,p}^F|\, d_{i,p}^F}{\chi(V_{i,p}^D)}, \qquad \hat q_{i,p}^F = \frac{|\gamma_{i,p}^F|}{d_{i,p}^F} \cot \omega_{i,p}. \tag{2.15}$$

If a neighbouring diamond cell $V_{i,p}^D$ is a boundary diamond cell (Fig. 2.3, right), we perform a substitution $T_{i,p}^n = F_{i,p}^n + F_{i,p+1}^n - T_i^n$ in equation (2.13).

2.2.6. Fully discrete formulation. The formulas (2.10), (2.13) represent a system of $3n_V = 3n_F + 3n_T$ linear equations for the (vector) unknowns F_i^n, $i = 1, \cdots, n_F$ and T_i^n, $i = 1, \cdots, n_T$. The system is coupled with an initial condition $F_i^0 = \varphi^0(X_i)$ and $T_i^0 = \varphi^0(B_i)$.

3. Numerical experiments. In this section we test the numerical scheme in several numerical experiments. In our implementation the BiCGStab (BiConjugate Gradient Stabilized) method [10] was used to solve the system of linear equations. In all experiments we set the initial position of each T-vertex to be a projection of the barycenter to the sphere with mean curvature vector equal to $\frac{1}{3}\left(h_{i,1}^F + h_{i,2}^F + h_{i,3}^F\right)$, where $h_{i,p}^F$ is the mean curvature vector in the neighbouring vertex $F_{i,p}$.

3.1. Experimental order of convergence. If the initial condition M^0 is the unit sphere, then the evolving surface M^t is a shrinking sphere with radius $r(t) = \sqrt{1-4t}$. The knowledge of the exact solution allows us to study the experimental order of convergence (EOC) of the numerical method. We calculate the EOC as

$$\mathrm{EOC} = \log_2 \left(\frac{\delta_h}{\delta_{h/2}} \right), \tag{3.1}$$

where δ_h is a space-time L_2-error for a mesh with characteristic edge length h.

We use the discretization of the sphere (Fig. 3.1) based on the division of the regular icosahedron. The mesh refinement was done by dividing each triangle into four triangles and the new F-vertices were projected onto the sphere. The stopping

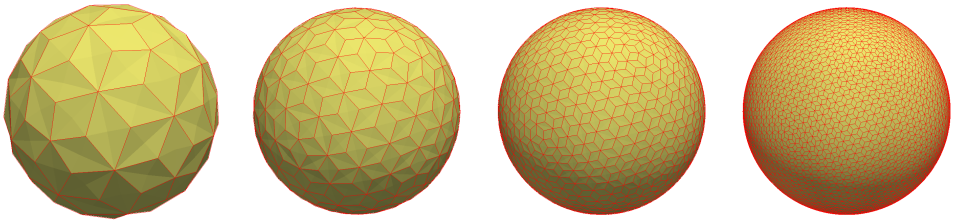

FIG. 3.1. *The discretization of the unit sphere for the DDFV method, from left to right:* $n_V = 122, 482, 1922, 7682$.

time was set to $t_f = 0.08\,\mathrm{s}$. We adopted the standard coupling for parabolic problems $\tau \sim h^2$. We use following L_2-error

$$L_2\text{-error} = \left[\sum_{n=1}^{N}\left(\sum_{i=1}^{n_F}\left(\|F_i^n\| - r(t^n)\right)^2 \frac{\chi^n(V_i^F)}{2} + \sum_{i=1}^{n_T}\left(\|T_i^n\| - r(t^n)\right)^2 \frac{\chi^n(V_i^T)}{2}\right)\tau\right]^{\frac{1}{2}}. \tag{3.2}$$

The results are presented in Tab. 3.1.

TABLE 3.1

Results for the DDFV method on sphere. n_V *is the total number of vertices,* n_F, n_T *denote the number of* F *and* T*-vertices respectively,* τ *is the time step,* N *is the number of time steps, next column is the* L_2 *error, "iter" is the total numbers of iterations of the BiCGStab method needed throughout the computation, EOC is the experimental order of convergence and CPU is the time in seconds needed for the computation on a single 2.3 GHz processor.*

n_V	n_F	n_T	τ	N	L_2error	iter	EOC	CPU
122	42	80	0.04	2	1.34e-02	7		0.02
482	162	320	0.01	8	3.26e-03	34	2.03	0.13
1922	642	1280	0.0025	32	8.01e-04	128	2.03	1.16
7682	2562	5120	0.00062500	128	1.95e-04	450	2.04	12.91
30722	10242	20480	0.00015625	512	4.66e-05	1703	2.07	194.78

Looking at Tab. 3.1 we observe the second order accuracy (EOC ≈ 2). This order of convergence is due to the space discretization that is second order accurate and due to the coupling $\tau \approx h^2$. Investigating the convergence in time alone, we would observe the first order accuracy.

3.2. The motion of T-vertices. The motion of T-vertices is crucial. A priori it is not clear if T-vertices will evolve properly with F-vertices and if the projection of

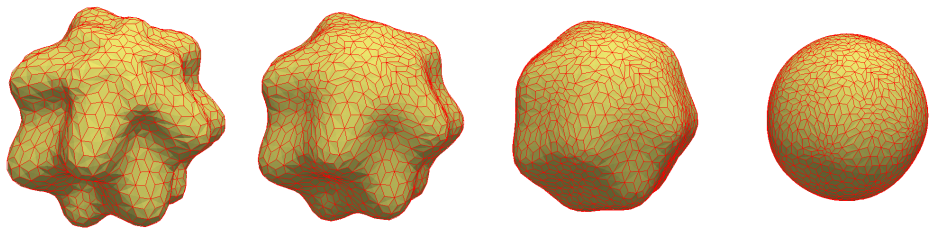

FIG. 3.2. *The evolution of a bumpy sphere with* $n_V = 1922$, $\tau = 0.0025$. *The selected time steps are* $n = 0, 4, 12, 32$.

T_i^n onto the plane of the triangle with vertices $F_{i,1}^n, F_{i,2}^n, F_{i,3}^n$ will lie in the triangle or if T-vertices can escape. In this section we test the behaviour of T-vertices for several initial conditions $\bar{M}^0$. The first example is the evolution of a bumpy sphere (Fig. 3.2). Looking at Fig. 3.2 we do not observe any undesirable behaviour of T-vertices (e.g. escaping). The second example is the evolution of a cymling-like shape (Fig. 3.3). We can observe that the regions with relatively high initial curvature become problematic during the evolution. In the detail in Fig. 3.4 we can see the contraction of diamond cells which would lead to obviously wrong results in the following time steps. This

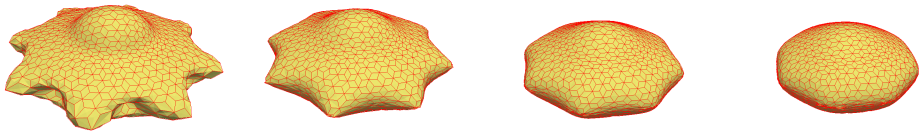

FIG. 3.3. *The evolution of a cymling-like shape with* $n_V = 1922$. *Time steps:* $n = 0, 4, 8, 12$.

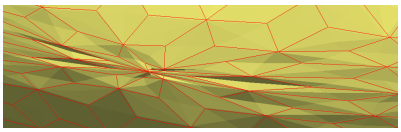

FIG. 3.4. *Contraction of diamond cells in the region of relatively high initial curvature.*

behaviour is also present in the cotangent scheme, where it can be eliminated by adding a special tangential term to the model (1.1) in order to control the tangential motion of the grid points [7]. The tangential redistribution of the grid points along the surface in the DDFV method could be the object of a further research.

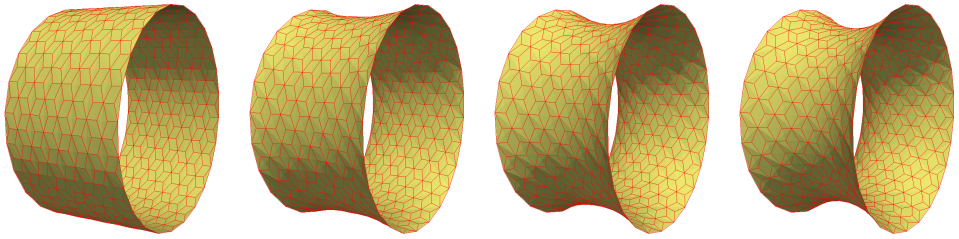

FIG. 3.5. *The evolution of a cylinder with* $n_V = 600$, $\tau = 0.0025$ *with diamond mesh displayed. The selected time steps are* $n = 0, 40, 100, 200$.

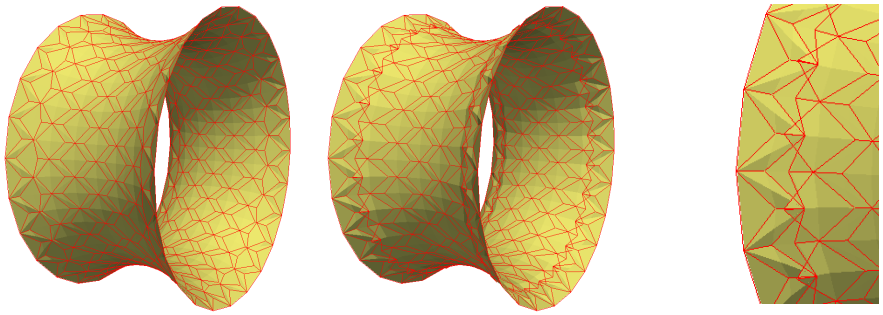

FIG. 3.6. *A degeneration of the diamond mesh. Left and middle, time steps* $n = 580, 640$. *Right, the degeneration in detail* $n = 640$.

The last example is the evolution of a cylinder with the Dirichlet boundary condition prescribed on the boundary circles. The evolving surface converges to the catenoid which is the minimal surface stretched between two circles (Fig. 3.5). However, at much later time steps we can observe an unwanted tangential motion of T-vertices and a degeneration of the diamond mesh (Fig. 3.6).

3.3. Eliminating the tangential velocity. In the numerical experiment with a cylinder evolving to the catenoid we revealed an unwanted tangential motion of T-vertices. Our basic model is the mean curvature flow $\partial_t\varphi = h$. We can rewrite the model into the form

$$\partial_t\varphi \cdot N = h \cdot N, \qquad (\partial_t\varphi \cdot T_1)T_1 + (\partial_t\varphi \cdot T_2)T_2 = 0, \tag{3.3}$$

where T_1, T_2 are vectors tangent to the surface and the vectors T_1, T_2, N form an orthonormal basis at each point of the surface. From the analytical point of view, the form (3.3) is equivalent to the basic model. However, the forms differ in the discrete setting. The mean curvature vector $h = HN$ is replaced by the Laplace-Beltrami operator $h = \triangle_\varphi\varphi$ and after discretization, the vector $\triangle_\varphi\varphi$ does not necessarily point in the normal direction, due to distretization errors. There are many possible ways of discretizing (3.3). We use the one presented below. Using (3.3) we obtain

$$\partial_t\varphi = (\partial_t\varphi \cdot N)N + \sum_{i=1}^{2}(\partial_t\varphi \cdot T_i)T_i = (\triangle_\varphi\varphi \cdot N)N. \tag{3.4}$$

In equation (3.4) the total velocity vector $\partial_t\varphi$ points in the normal direction, because the vector $\triangle_\varphi\varphi$ is projected onto the normal. Therefore, any tangential motion is prohibited. Before the discretization we add a zero to the right-hand side of (3.4).

$$\partial_t\varphi = \triangle_\varphi\varphi - \big(\triangle_\varphi\varphi - (\triangle_\varphi\varphi \cdot N)N\big) = \triangle_\varphi\varphi - \big(h - (h \cdot N)N\big). \tag{3.5}$$

The term $\big(h - (h \cdot N)N\big)$ represents the tangential velocity. The time discretization is performed using semi-implicit approach.

$$\frac{\varphi^n - \varphi^{n-1}}{\tau} = \triangle_{\varphi^{n-1}}\varphi^n - \big(h^{n-1} - (h^{n-1} \cdot N^{n-1})N^{n-1}\big). \tag{3.6}$$

After the space discretization we would obtain the system of equations similar to (2.10), (2.13), the difference would be in the right-hand side only.

In following experiments (Fig. 3.7 and Fig. 3.8) we can see that after elimination of the tangential velocity the T-vertices move properly and no degeneration of the diamond mesh is present.

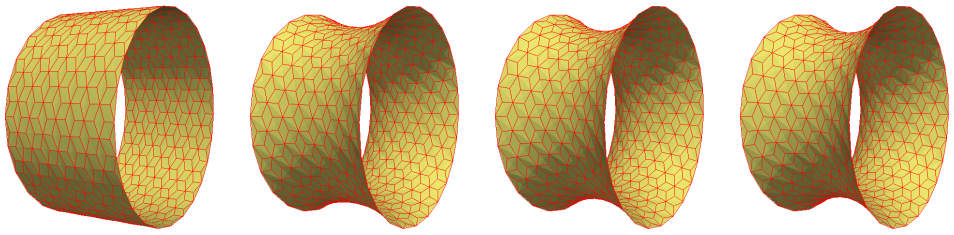

FIG. 3.7. *The evolution of a cylinder. No degeneration of the mesh is present. The selected time steps are* $n = 0, 100, 200, 640$.

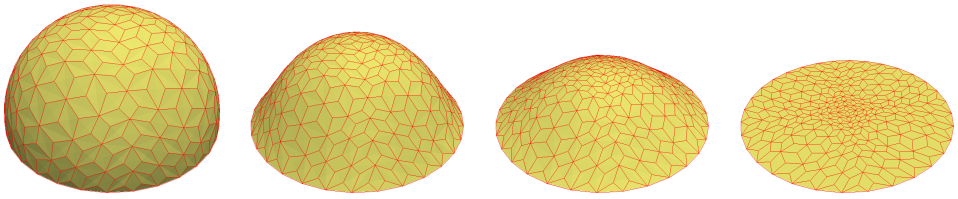

FIG. 3.8. *The evolution of a hemisphere. The selected time steps are* $n = 0, 40, 80, 600$.

REFERENCES

[1] J. W. Barrett, H. Garcke and R. Nurnberg, *On the parametric finite element approximation of evolving hypersurfaces in R^3*, J. Comput. Phys., 227 (2008), pp. 42814307.

[2] Y. Coudire, J.-P. Vila and P. Villedieu, *Convergence rate of a finite volume scheme for a two dimensional convection-diffusion problem.* ESAIM: M2AN 33 (1999) 493516.

[3] K. Domelevo and P. Omnes, *A finite volume method for the laplace equation on almost arbitrary two-dimensional grids.*, M2AN, 39(6):1203-1249, 2005.

[4] G. Dziuk and C.M. Elliot, *Finite elements on evolving surfaces*, IMA J. Numer. Anal. 27 (2007), pp. 262-292.

[5] R. Eymard, T. Gallout and R. Herbin, *Handbook of Numerical Analysis Vol. 7*, P.G. Ciarlet and J.-L. Lions, Eds., North- Holland/Elsevier, Amsterdam (2000) 7131020.

[6] C. Mantegazza, *Lecture Notes on Mean Curvature Flow*, Addison-Wesley publishing company, Birkhauser Verlag, (2011), 166 s. ISBN 978-3-0348-0144-7

[7] K. Mikula, M. Remešíková, P. Sarkoci and D. Ševčovič, *Manifold evolution with tangential redistribution of points*, SIAM J. Scientific Computing, Vol. 36, No.4 (2014), pp. A1384-A1414

[8] M. Meyer, M. Desbrun , P. Schroeder and A.H. Barr, *Discrete differential geometry operators for triangulated 2-manifolds*, Visualization and Mathematics III (H.-C. Hege and K. Polthier, eds.) (2003), pp. 35-57

[9] L. Tomek, *Discrete duality finite volume method for mean curvature flow of surfaces*, Project of PhD thesis. (2015)

[10] H. A. Van der Vorst, *Bi-CGSTAB: A fast and smoothly converging variant of Bi-CG for the solution of nonsymmetric linear systems*, SIAM J. Sci. Statist. Comput., 13 (1992), pp. 631644.